preadipocytes, knockdown of *Mkl1* expression (Supplementary Fig. 5a) resulted in a marked increase both in the expression of PPARγ and PPARγ target genes as well as in the extent of lipid droplet accumulation (Fig. 4a; Supplementary Fig. 5b,c). Moreover, we found that depletion of MKL1 alone resulted in a marked increase in the expression of PPARγ and PPARγ target genes even in NIH 3T3 nonadipogenic fibroblasts (Fig. 4b; Supplementary Fig. 5a). These findings indicated that loss of MKL1 function elicits PPARγ expression and adipocyte differentiation *in vitro*.

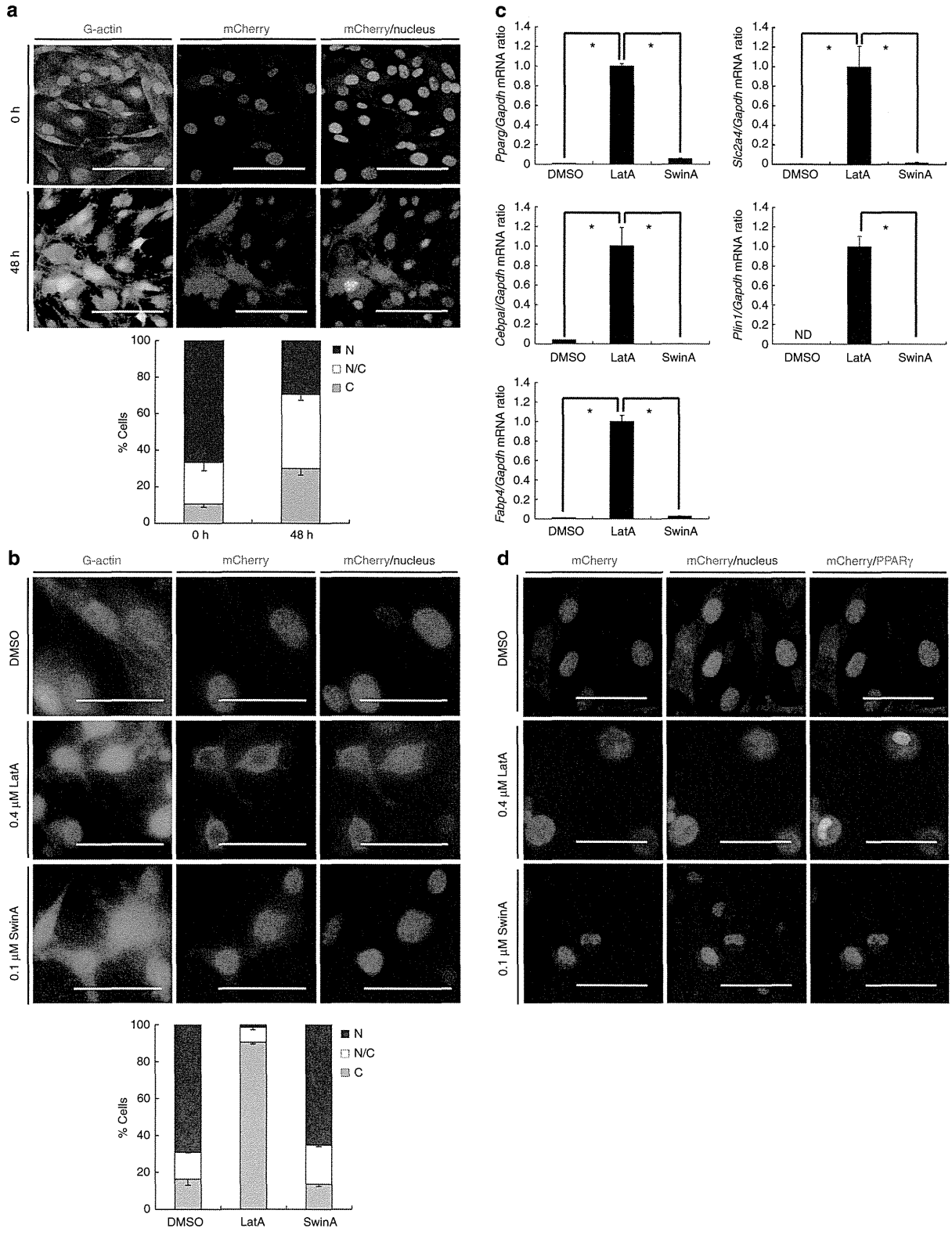

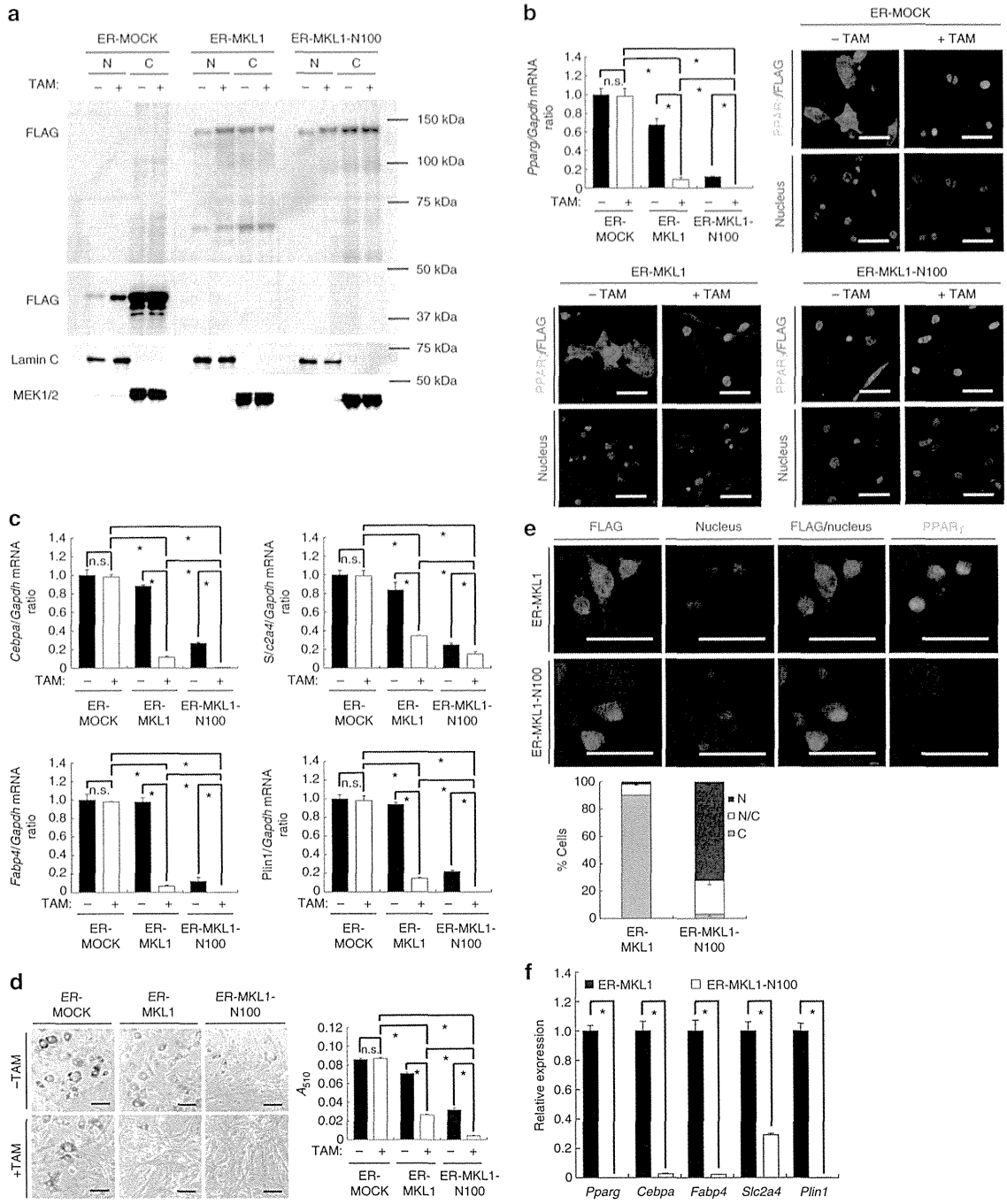

Figure 3 | Interaction between G-actin and MKL1 and the consequent cytoplasmic sequestration of MKL1 are required for adipocytic differentiation in DFAT cells. (**a**) Cells stably expressing 3 × FLAG-tagged ER (ER-MOCK, control), ER-MKL1 or ER-MKL1-N100 were exposed for 48 h to inducers of adipogenic differentiation in the absence or presence of TAM (1 μM), after which nuclear (N) and cytoplasmic (C) fractions were prepared from the cells and subjected to immunoblot analysis of FLAG, lamin C (nuclear marker) and MEK1/2 (cytoplasmic marker). (**b**) Cells treated as in **a** were analysed for the relative abundance of *Pparg* mRNA or subjected to immunofluorescence analysis of FLAG and PPARγ. Nuclei were stained with Hoechst 33342. Scale bars, 50 μm. (**c**) Relative abundance of *Cebpa*, *Fabp4*, *Slc2a4* and *Plin1* mRNAs in cells treated as in **a**. (**d**) Cells treated as in **a** were cultured for an additional 48 h (total of 96 h) and then stained with oil red O. Scale bars, 100 μm. The A_{510} of dye extracted from the stained cells was also determined. n.s., not significant. (**e**) Cells stably expressing ER-MKL1 or ER-MKL1-N100 were exposed for 24 h to Lat A (0.4 μM) in the presence of TAM (1 μM) and then subjected to immunofluorescence analysis of FLAG and PPARγ (upper panels). Nuclei were stained with Hoechst 33342. Scale bars, 50 μm. At least 300 cells per coverslip were scored for determination of the percentage of the subcellular localization of MKL1 (centre panel). N, nuclear; N/C, comparable intensity in nucleus and cytoplasm; C, cytoplasmic. (**f**) Relative abundance of *Pparg*, *Cebpa*, *Fabp4*, *Slc2a4* and *Plin1* mRNAs in cells treated as in **e**. All quantitative data are means ± s.d. ($n = 3$ experiments). *$P < 0.05$, Student's *t*-test.

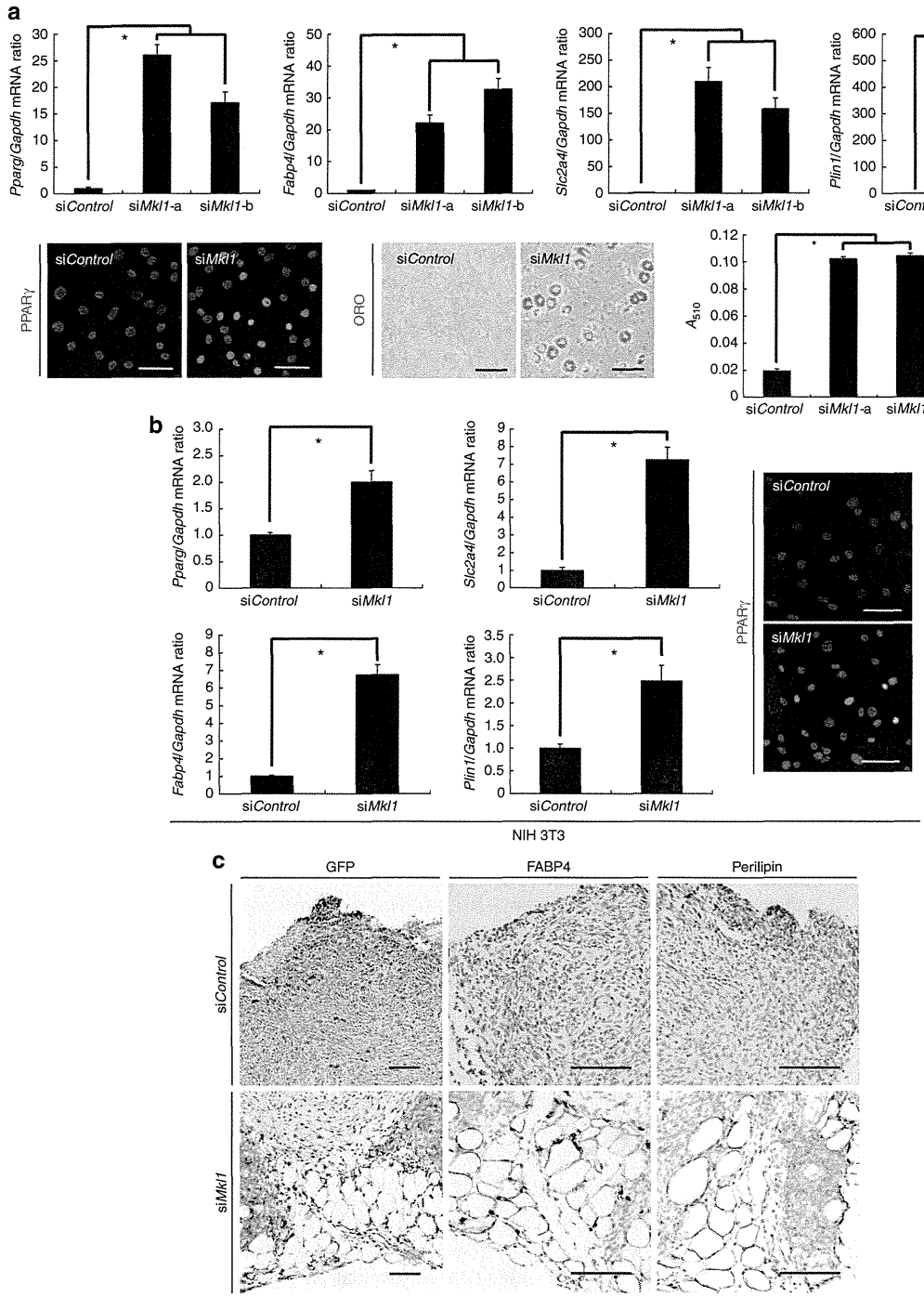

Figure 4 | Loss of MKL1 is sufficient to drive adipocyte differentiation *in vitro* and *in vivo*. (**a**) DFAT cells were transiently transfected with MKL1 (si*Mkl1*-a or -b) or control (si*Control*) siRNAs for 48 h and then cultured in growth medium without an adipogenic cocktail for 96 h, after which the relative abundance of *Pparg*, *Fabp4*, *Slc2a4* and *Plin1* mRNAs was determined (upper panels). The cells were also subjected to immunofluorescence analysis of PPARγ expression (bottom left panel). Nuclei were stained with Hoechst 33342. Scale bars, 100 μm. They were also stained with oil red O (bottom centre panel; Scale bars, 100 μm), and the A_{510} of dye extracted from the stained cells was determined (bottom right panel). (**b**) NIH 3T3 fibroblasts were transiently transfected with MKL1 (si*Mkl1*-a) or control siRNAs for 48 h and then cultured in growth medium without an adipogenic cocktail for 96 h, after which the relative abundance of *Pparg*, *Fabp4*, *Slc2a4*, and *Plin1* mRNAs was determined (left panels). The cells were also subjected to immunofluorescence analysis of PPARγ expression (right panel). Nuclei were stained with Hoechst 33342. Scale bars, 100 μm. (**c**) DFAT cells were transiently transfected with MKL1 (si*Mkl1*-a) or control siRNAs for 48 h and then injected subcutaneously into mice. Serial sections of the injection site were subjected to immunohistochemical staining of GFP (to identify injected cells) as well as of FABP4 and perilipin (markers of terminal adipogenic differentiation) at 2 weeks after injection. The sections were counterstained with hematoxylin. Data are representative of five mice per group. Scale bars, 100 μm. All quantitative data are means ± s.d. ($n = 3$ experiments). *$P < 0.05$, Student's *t*-test.

To investigate the function of MKL1 in adipocyte differentiation *in vivo*, we transfected DFAT cells (which are derived from green fluorescent protein (GFP) transgenic mice)[12] with MKL1 siRNA for 48 h (resulting in a significant decrease in *Mkl1* expression but no change in *Pparg* expression at this time (Supplementary Fig. 5d)) and then injected the cells subcutaneously into mice. At 2 weeks after injection, many fully differentiated adipocytes were observed at the injection site in the animals that received cells transfected with MKL1 siRNA but not in those that received cells transfected with a control siRNA (Fig. 4c). The transplanted MKL1-depleted cells were thus strongly positive for markers of terminal adipogenic differentiation (FABP4 and perilipin) as well as for GFP (Fig. 4c). Together, these data revealed that MKL1 functions as a gatekeeper that controls adipocyte differentiation both *in vitro* and *in vivo*. It was previously reported that the postpartum mammary glands of Mkl1 knockout female mouse show premature involution and markedly increased white adipose tissue[34]. This phenotype of Mkl1 knockout mouse is concordant with our finding that loss of Mkl1 promotes adipocyte differentiation programme.

We also performed microarray analysis to examine the gene expression profile of cells treated with ROCK inhibitor (Y-27632) or depleted MKL1 expression by siRNA (siMkl1) and functional classification of highly expressed genes (>2-fold). The gene ontology (GO) analysis revealed the most significant biological function was 'fat cell differentiation' (GO:0045444) in both ROCK inhibition and MKL1 knockdown (Table 1). Furthermore, hierarchical clustering of all samples for 133 fat cell differentiation-associated genes demonstrated an extremely high similarity of the gene expression pattern between Y-27632 sample and siMkl1 sample (Supplementary Fig. 6a), suggesting that either ROCK inhibition or MKL1 knockdown alone predominantly induces the expression of adipocyte differentiation-associated genes in global gene expression level. Furthermore, we extracted the expression patterns of a large number of well-documented serum response factor (SRF)-MKL1 target genes[26] from those microarray data. The relative expression of these SRF-MKL1 target genes tends to decrease on ROCK inhibition and MKL1 knockdown (Supplementary Fig. 6b), suggesting that either ROCK inhibition or MKL1 knockdown in common suppresses the expression of genes downstream of MKL1.

Table 1 | Gene ontology classifications for the highly expressed genes in ROCK inhibitor or MKL1 knockdown.

Gene Ontology class (Biological process with GO ID)	No. of genes in class	B-H *P*-value
Y-27632>DMSO (160 genes)		
GO:0045444—fat cell differentiation	14	1.57E-10
GO:0050873—brown fat cell differentiation	10	1.31E-08
GO:0050896—response to stimulus	58	4.69E-06
GO:0006629—lipid metabolic process	26	7.94E-05
GO:0002526—acute inflammatory response	10	8.33E-05
siMkl1>siControl (213 genes)		
GO:0045444—fat cell differentiation	19	7.26E-16
GO:0050873—brown fat cell differentiation	15	8.58E-16
GO:0006629—lipid metabolic process	33	6.41E-06
GO:0044255—cellular lipid metabolic process	27	5.40E-06
GO:0002526—response to hormone stimulus	16	7.75E-06

GO analysis were performed individually on the highly expressed genes (>2-fold) in Y-27632 sample (160 genes) or in siMkl1 sample (213 genes). All functional categories demonstrated enhanced statistical representation.

PPARγ induces *Mkl1* downregulation during adipogenesis. We noticed that treatment with Y-27632, which elicited remodelling of the actin cytoskeleton, not only prevented nuclear translocation of MKL1 but also induced a significant decrease in the amount of *Mkl1* mRNA in DFAT cells and 3T3-L1 preadipocytes (Supplementary Fig. 3i). Moreover, we found that *Mkl1* expression correlated inversely with *Pparg* expression during adipocytic differentiation (Fig. 5a). To test whether PPARγ contributes to *Mkl1* downregulation during adipogenesis, we investigated the effect of PPARγ knockdown on *Mkl1* expression. We established DFAT cells stably depleted of PPARγ as a result of retrovirus-mediated expression of a specific short hairpin RNA (shRNA) (Fig. 5b). Although control cells expressing a luciferase shRNA manifested a significant decrease in the abundance of *Mkl1* mRNA after exposure to inducers of adipocytic differentiation, cells expressing the PPARγ shRNA did not (Fig. 5b). To clarify further the influence of PPARγ on *Mkl1* expression, we generated DFAT cells that stably overexpress PPARγ (Fig. 5c). Overexpression of PPARγ resulted in a significant decrease in the amount of *Mkl1* mRNA (Fig. 5c), indicating that PPARγ indeed suppresses the expression of *Mkl1*, resulting in the continuous activation of PPARγ required for the completion of adipocyte differentiation.

Discussion

On the basis of our observations, we propose a model for the control of adipocyte differentiation in which regulation of MKL1 by disruption of actin stress fibres triggers the differentiation programme (Fig. 5d). Exposure of preadipocytes to an adipogenic cocktail results in the rapid disruption of actin stress fibres as a consequence of downregulation of RhoA-ROCK signalling. The resulting increase in the amount of G-actin leads to the binding of G-actin to MKL1 and to inhibition of the nuclear translocation and transcriptional regulatory activity of the latter protein. Transcription of the *Pparg* gene is thereby activated, and the encoded protein then mediates not only upregulation of the expression of genes (such as *Fabp4*, *Plin* and *Slc2a4*) associated with the adipocyte phenotype but also downregulation of *Mkl1* expression to allow completion of adipogenesis.

Several preadipocyte cell lines undergo differentiation on treatment with a standard adipogenic cocktail consisting of IBMX, dexamethasone and insulin[35]. Both IBMX and dexamethasone trigger the activation of protein kinase A by increasing the intracellular concentration of cAMP, thereby promoting adipocyte differentiation[36]. The major role of protein kinase A in adipogenesis has been thought to lie in downregulation of RhoA and ROCK activity[37]. In the present study, we found that Rho activity is rapidly reduced after treatment of DFAT cells with the adipogenic cocktail, and the downregulation of RhoA-ROCK signalling then promotes adipocyte differentiation via modulation of remodelling of the actin cytoskeleton. In addition, we found that treatment with LatA alone or Y-27632 alone, by inducing remodelling of the actin cytoskeleton, is sufficient to trigger adipocyte differentiation in the absence of an adipogenic cocktail. Our findings, combined with previous observations, thus suggest that a standard adipogenic cocktail directly elicits reorganization of the actin cytoskeleton through downregulation of RhoA-ROCK signalling, and that the disruption of actin stress fibres then acts as a trigger for the adipocytic differentiation of preadipocytes *in vitro*.

In differentiated adipocytes, cortical F-actin has an important regulatory role in the insulin-stimulated translocation of the glucose transporter GLUT4 (encoded by *Slc2a4*) from intracellular storage sites to the plasma membrane[10], with the formation of cortical F-actin thus likely being a key event in adipogenesis.

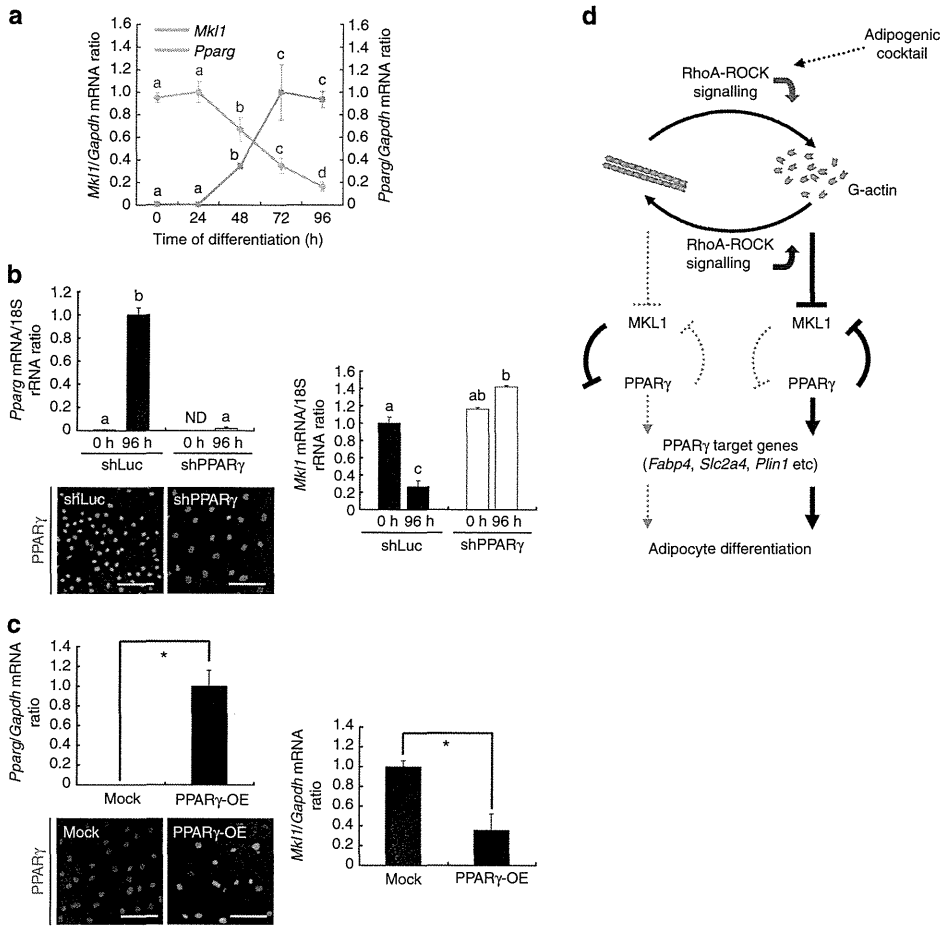

Figure 5 | PPARγ contributes to *Mkl1* downregulation during adipocyte differentiation. (**a**) The relative abundance of *Mkl1* and *Pparg* mRNAs at the indicated times after exposure of DFAT cells to inducers of adipocytic differentiation was also determined. (**a-c**) $P<0.05$, (**a-d**) $P<0.05$, Tukey's honest significant difference test. (**b**) DFAT cells stably expressing PPARγ (shPPARγ) or luciferase (shLuc, control) shRNAs were exposed to inducers of adipogenesis for 0 or 96 h and then assayed for the relative abundance of *Pparg* and *Mkl1* mRNAs. The cells were also subjected to immunofluorescence analysis of PPARγ after 96 h. Nuclei were stained with Hoechst 33342. Scale bars, 100 μm. ND, not detected. (**c**) DFAT cells stably overexpressing PPARγ (PPARγ-OE) or infected with the corresponding empty vector (Mock) were assayed for the relative abundance of *Pparg* and *Mkl1* mRNAs. *$P<0.05$, Student's *t*-test. They were also subjected to immunofluorescence analysis of PPARγ expression. Nuclei were stained with Hoechst 33342. Scale bars, 100 μm. All quantitative data are means ± s.d. ($n=3$ experiments). (**d**) Model for the regulation of adipocyte differentiation. Regulation of MKL1 by disruption of actin stress fibres drives adipocyte differentiation.

In the present study, F-actin stress fibres were depolymerized to G-actin within 24 h after the induction of adipocyte differentiation, and the actin cytoskeleton was subsequently reorganized to form cortical F-actin structures within 48 h. The abundance of transcripts for MKL1, which binds to G-actin, began to decline within 48 h after induction of adipocyte differentiation, and this downregulation of *Mkl1* was controlled by PPARγ. We also found that cells depleted of PPARγ maintained a high level of *Mkl1* expression even after induction of adipocyte differentiation, and that these cells manifested disruption of actin stress fibres at 24 h but not the formation of cortical F-actin structures even at 96 h (Supplementary Fig. 4e). Together, these observations suggest that the downregulation of *Mkl1* expression not only contributes to the continued activation of PPARγ but also promotes the organization of adipocyte-specific cortical F-actin structures as a result of the release of G-actin from MKL1–G-actin complexes.

Our findings provide new insight into the regulatory mechanism of adipocyte differentiation, which is shown to be triggered through regulation of MKL1 resulting from disruption of actin stress fibres. They also identify MKL1 as a novel gatekeeper in the regulation of adipogenesis as well as provide a basis for further studies of the relation between the dynamics of cell shape and transcription factor function during cellular differentiation. Lastly, given that activating mutations of RAC protein, which belongs to the RHO family of small GTPases and orchestrates actin polymerization, were found in a wide variety of human cancers and given their marked transforming ability[38], we assume that aberrant differentiation associated with actin cytoskeleton dynamics can be a critical factor of tumorigenesis, and our works thus would potentially contribute to understanding cancer biology.

Methods

Cell culture. The mouse preadipocyte cell line DFAT was established from dedifferentiated mature adipocytes of GFP transgenic mice by ceiling culture (a method to culture lipid-containing adipocytes based on their lipid buoyancy)[12]. The mouse embryonic preadipocyte cell line 3T3-L1 and the mouse embryonic fibroblast cell line NIH 3T3 were obtained from the Japanese Collection of Research Bioresources (Tokyo, Japan). DFAT, 3T3-L1, or NIH 3T3 cells were cultured under a humidified atmosphere of 5% CO_2 and 95% air at 37 °C on glass

coverslips (Matsunami, Osaka, Japan) placed in tissue culture dishes (Falcon 3001; BD, Bedford, MA) containing Dulbecco's modified Eagle's medium (DMEM) (Nissui Pharmaceutical, Tokyo, Japan) supplemented with 10% fetal bovine serum (FBS) (Moregate BioTech, Bulimba, Queensland, Australia). DFAT or 3T3-L1 cells were grown to semiconfluence before induction of differentiation by exposure to DMEM supplemented with FBS (1% or 10%, respectively), 0.5 mM IBMX (Wako, Osaka, Japan), 0.1 μM dexamethasone (Wako), and insulin-transferrin-selenium-X supplement (final insulin concentration of 5 μg ml^{-1}) (Invitrogen, Carlsbad, CA).

Time-lapse imaging. For time-lapse observation of actin dynamics during adipocyte differentiation, DFAT cells were infected with Cellular Lights Actin-RFP baculovirus expression vectors (Invitrogen) and then cultured in a glass-bottomed dish (Iwaki, Chiba, Japan). After the cells achieved semiconfluence, adipocyte differentiation was induced as described above and time-lapse fluorescence and differential interference contrast video microscopy was performed with the use of a microscope (Olympus LCV110) equipped with an incubation chamber. Images were acquired every 30 min with the use of a charge-coupled device camera (Retiga Exi, QImaging) equipped with a U Plan Super Apochromatic ×40, 0.95 numerical aperture objective and were analysed with MetaMorph software (Molecular Devices, Sunnyvale, CA).

RT and real-time PCR analysis. Total RNA was isolated from cells with the use of the Trizol reagent (Invitrogen), and portions (1 μg) of the DNase I–treated RNA were subjected to reverse transcription (RT) with the use of high-capacity RNA-to-cDNA master mix (Applied Biosystems, Foster City, CA). The probes for PPARγ (*Pparg*; GenBank accession no. NM_011146.3; Mm00440940_m1), C/EBPα (*Cebpa*; GenBank accession no. NM_007678.3; Mm00514283_s1), fatty acid-binding protein 4 (*Fabp4*; GenBank accession no. NM_024406.2; Mm00445878_m1), GLUT4 (*Slc2a4*; GenBank accession no. NM_009204.2; Mm01245502_m1), perilipin 1 (*Plin1*; GenBank accession no. NM_175640.2; Mm00558672_m1) and MKL1 (*Mkl1*; GenBank accession no. NM_153049.2; Mm00461840_m1) genes were obtained fromTaqMan Pre-Developed Assay Reagents (Applied Biosystems). A mouse glyceraldehyde-3-phosphate dehydrogenase (*Gapdh*; GenBank accession no. NM_008084.2) TaqMan probe (4352339E, Applied Biosystems) or eukaryotic 18S rRNA (GenBank accession no. X03205.1) TaqMan probe (4319413E, Applied Biosystems) was included as an endogenous control. The RT products (2 μl) were subjected to real-time PCR analysis in a final volume of 10 μl with the use of TaqMan Fast Universal PCR master mix (Applied Biosystems) and with an ABI7500 thermocycler. Each sample was assayed in triplicate.

Immunoblot analysis. Cells were washed extensively with phosphate-buffered saline (PBS) and then either recovered directly with a rubber scraper in SDS sample buffer (62.5 mM Tris-HCl (pH 6.8), 10% SDS, 5% glycerol, 5% β-mercaptoethanol, 10% bromophenol blue) or subjected to extraction of nuclear and cytoplasmic fractions with the use of an NE-PER nuclear and cytoplasmic extraction reagent kit (Pierce, Rockford, IL). Samples were subjected to SDS–polyacrylamide gel electrophoresis, the separated proteins were transferred electrophoretically to a polyvinylidene difluoride membrane (Millipore, Bedford, MA), and nonspecific sites of the membrane were then blocked by incubation with Blocking One (Nacalai Tesque, Kyoto, Japan) for 1 h at room temperature. The membrane was then exposed for 24 h at 4 °C to rabbit polyclonal antibodies to PPARγ (1:500 dilution; P0744; Sigma-Aldrich, St Louis, MO), to lamin A/C (1:500 dilution; #2032; Cell Signalling Technology, Beverly, MA), or to MEK1/2 (1:500 dilution; #9122; Cell Signalling Technology); rabbit monoclonal antibodies to cofilin (1:1,000 dilution; #5175; Cell Signalling Technology); or mouse monoclonal antibodies to FLAG (1:1,000 dilution; F1804; Sigma-Aldrich), to GAPDH (1:10,000 dilution; G8795; Sigma-Aldrich), or to α-tubulin (1:10,000 dilution; T5168; Sigma-Aldrich). The membrane was washed with PBS containing 0.02% Tween 20, incubated for 1 h at room temperature with horseradish peroxidase–conjugated goat antibodies to rabbit or mouse immunoglobulin G (1:2,000 dilution; GE Healthcare, Tokyo, Japan), and washed again with PBS containing 0.02% Tween 20, after which immunoreactive proteins were visualized with the use of enhanced chemiluminescence reagents (GE Healthcare). Uncropped scans of the most important western blots were shown in Supplementary Fig. 7.

Immunofluorescence staining. Cells were fixed overnight at 4 °C in zinc fixative solution (0.1 M Tris-HCl (pH 7.4), calcium acetate (475 μg ml^{-1}), zinc acetate (5 mg ml^{-1}) and $ZnCl_2$ (5 mg ml^{-1}) in ultrapure water) containing 0.2% Triton X-100. They were then washed in Tris-buffered saline (TBS) and incubated for 1 h at room temperature with 10% normal goat or horse serum (Vector Laboratories, Burlingame, CA) and 1% bovine serum albumin (BSA) (Sigma-Aldrich) in TBS to block nonspecific binding of antibodies before staining with primary antibodies according to standard procedures. Primary antibodies included rabbit monoclonal antibodies to PPARγ (1:200 dilution; #2435; Cell Signalling Technology); rabbit polyclonal antibodies to perilipin A/B (1:1,000 dilution; P1873; Sigma-Aldrich) and to MKL1 (1:100 dilution; ab49311; Abcam, Cambridge, MA); and mouse monoclonal antibodies to β-actin (1:1,000 dilution; A5441; Sigma-Aldrich), to HA (1:500 dilution; 1583816; Roche, Mannheim, Germany), and to FLAG (1:1,000 dilution; F1804; Sigma-Aldrich). Immune complexes were detected with Alexa Fluor 488– or Alexa Fluor 594–conjugated goat antibodies to rabbit or mouse immunoglobulin G (each at 1:2,000 dilution; Molecular Probes, Eugene, OR). Antibodies were diluted in TBS containing 1% BSA. F-actin was stained with Alexa Fluor 488– or Alex Fluor 594–labelled phalloidin (Molecular Probes) at 200 U ml^{-1} in TBS, and G-actin was stained with Alexa Fluor 594–labelled DNase I (Molecular Probes) at 9 μg ml^{-1} in TBS. Cells were counterstained with Hoechst 33342 (Sigma-Aldrich) at 5 μg ml^{-1} in TBS and were observed with a laser-scanning confocal microscope (Olympus FV-750) and a BIOREVO BZ-9000 fluorescence microscope (Keyence, Osaka, Japan).

Lipid staining. Lipid accumulation in adipocytes was detected by staining with oil red O (Wako). Cells were washed three times with PBS, fixed for 1 h at room temperature with 10% formalin in phosphate buffer, washed again with PBS and stained for 15 min at room temperature with a filtered solution of oil red O (0.5 g in 100 ml of isopropyl alcohol). The cells were then washed twice with distilled water for 15 min. For quantitation of lipid accumulation, dimethyl sulfoxide (DMSO) (500 μl per 35-mm dish) was added to the washed and dried cells for 1 min, after which the absorbance of the extracted dye at 510 nm was measured with a spectrophotometer (ND-1000; Nanodrop Technologies, Wilmington, DE) and was normalized by dish area.

Pharmacological agents. Cells were exposed to the following agents: 5 μM phalloidin oleate (Calbiochem, San Diego, CA) dissolved in DMSO, 30 μM Y-27632 (Calbiochem) dissolved in water, 0.2 μM cytochalasin D (CytD) (Sigma-Aldrich) dissolved in DMSO, 0.4 μM latrunculin A (LatA) (Calbiochem) dissolved in DMSO, 0.1 μM swinholide A (SwinA) (Calbiochem) dissolved in ethanol or 1 μM 4-hydroxytamoxifen (TAM) (Sigma-Aldrich) dissolved in ethanol.

Rho activation assay. Cells were lysed by incubation with a magnesium-containing buffer (25 mM HEPES-NaOH (pH 7.5), 150 mM NaCl, 1% Igepal CA-630 detergent, 10 mM $MgCl_2$, 1 mM EDTA, 2% glycerol) supplemented with 25 mM NaF, 1 mM Na_3VO_4, and a protease inhibitor cocktail (Nacalai Tesque). The lysates were centrifuged at 14,000 × *g* for 5 min at 4 °C, and the resulting supernatants were incubated for 45 min at 4 °C with 25 μg of a glutathione S-transferase fusion protein of the Rho-binding domain (amino acids 7–89) of rhotekin that was bound to glutathione-Sepharose beads (Millipore). The beads were washed three times with the magnesium-containing buffer and then subjected to immunoblot analysis with mouse monoclonal antibodies to RhoA, -B and -C (1:250 dilution; #05-778; Millipore). Whole-cell lysates were also subjected to immunoblot analysis with the antibodies to Rho and those to GAPDH (loading control).

Transplantation and histological evaluation. All animal studies were performed according to the NIH Guide for the Care and Use of Laboratory Animals. C57BL/6J mice were obtained from Oriental Yeast (Tokyo, Japan). DFAT cells (1×10^5) collected with the use of a cell scraper were injected subcutaneously with a syringe above the sternum of 10 female mice at 8 weeks of age. After 2 weeks, cells at the injection site were retrieved, fixed in paraformaldehyde and embedded in paraffin. For immunohistochemical analysis, tissue sections were depleted of paraffin, washed with TBS, and stained with the use of a Vectastain ABC kit (Vector Laboratories). Primary antibodies included rabbit polyclonal antibodies to GFP (1:100 dilution; sc-8334; Santa Cruz Biotechnology, Santa Cruz, CA), to FABP4 (1:1,000 dilution; ab13979; Abcam) and to perilipin A/B (1:1,000 dilution; P1873; Sigma-Aldrich). The sections were counterstained with hematoxylin (Wako).

Plasmid transfection. The plasmids pEF-BOS-HA-RhoAV14 and pEF-BOS-HA-RhoAN19 (ref. 39) plasmids were transfected into DFAT cells for 24 h using the Fugene HD reagent (Roche).

RNAi. Expression of shRNAs was achieved with the retroviral expression vector pRePS (kindly provided by T. Hara), which also contains a puromycin resistance gene. The sequences of the sense oligonucleotides were 5′-GTTTGAGTTTG CTGTGAAG-3′ for PPARγ shRNA[40] and 5′-CGTACGCGGAATACTTCGA-3′ for luciferase shRNA (nonspecific control). pReps vectors transfected into Plat-E packaging cells[41] using Fugene HD (Roche). Medium was replaced once after 24 h, and viral supernatants were collected and filtered with 0.45-μm cellulose acetate filters (Iwaki) 48 h after transfection. Retroviral infection was carried out in a six-well plate for 48 h, and infected cells were then subjected to selection in the presence of puromycin (10 μg ml^{-1}). The sequences of siRNAs targeting cofilin1 were 5′-GAUGAACACCAGGUCCUCCUU-3′ for *Cfl1*-a, 5′-AAGAUCAAAAG CAGUUUGGGA-3′ for *Cfl1*-b, and 5′-UCACUAUUGUGGUUAGAAGUU-3′ for *Cfl1*-c, and those of siRNAs targeting MKL1 were 5′-CGAGGACUAUUUGAAA CGGAA-3′ for *Mkl1*-a and 5′-CCCACUCAGGUUCUUUCUCAA-3′ for *Mkl1*-b. The control siRNA sequence was 5′-GCGCGCUUUGUAGGAUUCG-3′. Cells

were transfected with siRNA duplexes for 48 h with the use of Lipofectamine RNAiMAX (Invitrogen).

Retroviral gene transfer. The coding region for mCherry cDNA was amplified from the vector containing mCherry-MKlp2 (ref. 42) by PCR with the primers 5′-CCGCTCGAGATGGTGAGCAAGGGCGAGGAGGATAACATG-3′ (XhoI_mCherry forward primer) and 5′-CGGAATTCTTCTTGTACAGCT CGTCCATGCCGCCGGTGG-3′ (mCherry_EcoRI reverse primer), and the coding region for human ER was amplified from the pMV7-MycER plasmid[43] by PCR with the primers 5′-CCGCTCGAGTCTGCTGGAGACATGAGAGCTGCCAA CCTT-3′ (XhoI_ER forward primer) and 5′-CGGAATTCTTGACCGTGGCAG GGAAACCCTCTGCCTCCCC-3′ (ER_EcoRI reverse primer), digested with XhoI and EcoRI, and ligated into the XhoI and EcoRI sites of pMXs-3 × FLAG-IP[42]. Human cDNAs for full-length MKL1 and MKL1-N100 were obtained by digestion of Addgene Plasmids (#11978, #27176)[32] with EcoRI and BamHI, and the resulting fragments were cloned into the EcoRI and BamHI sites of pMXs-3 × FLAG-mCherry-IP and/or pMXs-3 × FLAG-ER-IP. The resulting vectors were designated pMXs-3 × FLAG-mCherry-MKL1-IP, pMXs-3 × FLAG-ER-MKL1-IP, or pMXs-3 × FLAG-ER-MKL1-N100-IP, and pMXs-3 × FLAG-mCherry-IP or pMXs-3 × FLAG-ER-IP was used as a control. Mouse PPARγ cDNA (ImaGenes, Berlin, Germany) was cloned into the retroviral plasmid pMXs-puro (kindly provided by T. Kitamura). pMXs vectors were transfected into Plat-E packaging cells[44] using FugeneHD (Roche). Medium was replaced once after 24 h, and viral supernatants were collected and filtered with 0.45-μm cellulose acetate filters (Iwaki) 48 h after transfection. Retroviral infection was carried out in a six-well plate for 48 h, and infected cells were subjected to selection in the presence of puromycin (10 μg ml^{-1}).

Microarray analysis. The quality of RNA was assessed using the Agilent 2100 Bioanalyzer (Agilent Technologies, Waldbronn, Germany). The RNA samples were labelled using the GeneChip One-Cycle Target Labeling and Control Reagent pakage (Affymetrix, Santa Clara, CA) and then hybridized to the Affymetrix GeneChip mouse genome 430 2.0 array according to the manufacturer's instruction. Fluorescent images were visualized using a GeneChip Scanner 3000 (Affymetrix). Expression and raw expression data (CEL files) were summarized and normalized using the Robust Multi-array Average algorithm and the Bioconductor package affy (http://www.bioconductor.org/packages/2.0/bioc/html/affy.html). The Spotfire DecisionSite for Functional Genomics software package (TIBCO Software, Palo Alto, CA) was used for visualization of microarray data. Functional analyses were performed using DAVID Bioinformatics Resources 6.7 (http://david.abcc.ncifcrf.gov/). Functional analysis identified the biological functions that were most significant to the data set.

Statistical analysis. Data are presented as means ± s.d. and were analysed with Tukey's honest significant difference test or Student's *t*-test for comparisons between two or among three or more groups, respectively. A *P*-value of <0.05 was considered statistically significant.

References

1. Braun, T. & Gautel, M. Transcriptional mechanisms regulating skeletal muscle differentiation, growth and homeostasis. *Nat. Rev. Mol. Cell Biol.* **12,** 349–361 (2011).
2. de Crombrugghe, B., Lefebvre, V. & Nakashima, K. Regulatory mechanisms in the pathways of cartilage and bone formation. *Curr. Opin. Cell Biol.* **13,** 721–727 (2001).
3. Farmer, S. R. Transcriptional control of adipocyte formation. *Cell Metab.* **4,** 263–273 (2006).
4. Wu, Z. *et al.* Cross-regulation of C/EBPα and PPARγ controls the transcriptional pathway of adipogenesis and insulin sensitivity. *Mol. Cell* **3,** 151–158 (1999).
5. Tontonoz, P., Hu, E. & Spiegelman, B. M. Stimulation of adipogenesis in fibroblasts by PPARγ2, a lipid-activated transcription factor. *Cell* **79,** 1147–1156 (1994).
6. Okuno, M., Arimoto, E., Nishizuka, M., Nishihara, T. & Imagawa, M. Isolation of up- or down-regulated genes in PPARγ-expressing NIH3T3 cells during differentiation into adipocytes. *FEBS Lett.* **519,** 108–112 (2002).
7. Rosen, E. D. & MacDougald, O. A. Adipocyte differentiation from the inside out. *Nat. Rev. Mol. Cell Biol.* **7,** 885–896 (2006).
8. Smas, C. M. & Sul, H. S. Control of adipocyte differentiation. *Biochem. J.* **309,** 697–710 (1995).
9. Jaffe, A. B. & Hall, A. Rho GTPases: biochemistry and biology. *Annu. Rev. Cell Dev. Biol.* **21,** 247–269 (2005).
10. Kanzaki, M. & Pessin, J. E. Insulin-stimulated GLUT4 translocation in adipocytes is dependent upon cortical actin remodeling. *J. Biol. Chem.* **276,** 42436–42444 (2001).
11. Noguchi, M. *et al.* Genetic and pharmacological inhibition of Rho-associated kinase II enhances adipogenesis. *J. Biol. Chem.* **282,** 29574–29583 (2007).
12. Nobusue, H., Endo, T. & Kano, K. Establishment of a preadipocyte cell line derived from mature adipocytes of GFP transgenic mice and formation of adipose tissue. *Cell Tissue Res.* **332,** 435–446 (2008).
13. Yagi, K., Kondo, D., Okazaki, Y. & Kano, K. A novel preadipocyte cell line established from mouse adult mature adipocytes. *Biochem. Biophys. Res. Commun.* **321,** 967–974 (2004).
14. Spiegelman, B. M. & Ginty, C. A. Fibronectin modulation of cell shape and lipogenic gene expression in 3T3-adipocytes. *Cell* **35,** 657–666 (1983).
15. McBeath, R., Pirone, D. M., Nelson, C. M., Bhadriraju, K. & Chen, C. S. Cell shape, cytoskeletal tension, and RhoA regulate stem cell lineage commitment. *Dev. Cell* **6,** 483–495 (2004).
16. Kilian, K. A., Bugarija, B., Lahn, B. T. & Mrksich, M. Geometric cues for directing the differentiation of mesenchymal stem cells. *Proc. Natl Acad. Sci. USA* **107,** 4872–4877 (2010).
17. Dupont, S. *et al.* Role of YAP/TAZ in mechanotransduction. *Nature* **474,** 179–183 (2011).
18. Cristancho, A. G. & Lazar, M. A. Forming functional fat: a growing understanding of adipocyte differentiation. *Nat. Rev. Mol. Cell Biol.* **12,** 722–734 (2011).
19. Ridley, A. J. & Hall, A. The small GTP-binding protein Rho regulates the assembly of focal adhesions and actin stress fibres in response to growth factors. *Cell* **70,** 389–399 (1992).
20. Riento, K. & Ridley, A. J. Rocks: multifunctional kinases in cell behaviour. *Nat. Rev. Mol. Cell Biol.* **4,** 446–456 (2003).
21. Hamm, J. K., El Jack, A. K., Pilch, P. F. & Farmer, S. R. Role of PPARγ in regulating adipocyte differentiation and insulin-responsive glucose uptake. *Ann. NY Acad. Sci.* **18,** 134–145 (1999).
22. Tashiro, K. *et al.* Efficient adenovirus vector-mediated PPARγ gene transfer into mouse embryoid bodies promotes adipocyte differentiation. *J. Gene Med.* **10,** 498–507 (2008).
23. Tontonoz, P. & Spiegelman, B. M. Fat and beyond: the diverse biology of PPARγ. *Annu. Rev. Biochem.* **77,** 289–312 (2008).
24. Qian, S. W. *et al.* Characterization of adipocyte differentiation from human mesenchymal stem cells in bone marrow. *BMC Dev. Biol.* **10,** 47 (2010).
25. Bamburg, J. R. Proteins of the ADF/cofilin family: essential regulators of actin dynamics. *Annu. Rev. Cell Dev. Biol.* **15,** 185–230 (1999).
26. Olson, E. N. & Nordheim, A. Linking actin dynamics and gene transcription to drive cellular motile functions. *Nat. Rev. Mol. Cell Biol.* **11,** 353–365 (2010).
27. Miralles, F., Posem, G., Zaromytidou, A. I. & Treisman, R. Actin dynamics control SRF activity by regulation of its coactivator MAL. *Cell* **113,** 329–342 (2003).
28. Vartiainen, M. K., Guettler, S., Larijiani, B. & Treisman, R. Nuclear actin regulates dynamic subcellular localization and activity of the SRF cofactor MAL. *Science* **316,** 1749–1752 (2007).
29. Yin, J. W. *et al.* Mediator MED23 plays opposing roles in directing smooth muscle cell and adipocyte differentiation. *Genes Dev.* **26,** 2192–2205 (2012).
30. Lyubimova, A., Bershadsky, A. D. & Ben-Ze'ev, A. Autoregulation of actin synthesis responds to monomeric actin levels. *J. Cell Biochem.* **65,** 469–478 (1997).
31. Bubb, M. R., Spector, I., Bershadsky, A. D. & Korn, E. D. Swinholide A is a microfilament disrupting marine toxin that stabilizes actin dimmers and severs actin filaments. *J. Biol. Chem.* **270,** 3463–3466 (1995).
32. Cen, B. *et al.* Megakaryoblastic leukemia 1, a potent transcriptional coactivator for serum response factor (SRF), is required for serum induction of SRF target genes. *Mol. Cell Biol.* **23,** 6597–6608 (2003).
33. Guettler, S., Vartiainen, M. K., Miralles, F., Larijani, B. & Treisman, R. RPEL motifs link the serum response factor cofactor MAL but not myocardin to Rho signaling *via* actin binding. *Mol. Cell Biol.* **28,** 732–742 (2008).
34. Sun, Y. *et al.* Acute myeloid leukemia-associated Mkl1 (Mrtf-a) is a key regulator of mammary gland function. *Mol. Cell Biol.* **26,** 5809–5826 (2006).
35. Liu, J. *et al.* Changes in integrin expression during adipocyte differentiation. *Cell Metab.* **2,** 165–177 (2005).
36. Vassaux, G., Gaillard, D., Ailhaud, G. & Négrel, R. Prostacyclin is a specific effector of adipose cell differentiation. Its dual role as a cAMP- and Ca^{2+}-elevating agent. *J. Biol. Chem.* **267,** 11092–11097 (1992).
37. Petersen, R. K. *et al.* Cyclic AMP (cAMP)-mediated stimulation of adipocyte differentiation requires the synergistic action of Epac- and cAMP-dependent protein kinase-dependent processes. *Mol. Cell Biol.* **28,** 3804–3816 (2008).
38. Kawazu, M. *et al.* Transforming mutations of RAC guanosine triphosphatases in human cancers. *Proc. Natl Acad. Sci. USA* **110,** 3029–3034 (2013).
39. Amano, M. *et al.* Identification of a putative target for Rho as the serine-threonine kinase protein kinase N. *Science* **271,** 648–650 (1996).
40. Shimizu, T. *et al.* c-MYC overexpression with loss of Ink4a/Arf transforms bone marrow stromal cells into osteosarcoma accompanied by loss of adipogenesis. *Oncogene* **29,** 5687–5699 (2010).

41. Fujino, R. S. *et al.* Spermatogonial cell-mediated activation of an IκBζ-independent nuclear factor-κB pathway in Sertoli cells induces transcription of the lipocalin-2 gene. *Mol. Endocrinol.* **20,** 904–915 (2006).
42. Kitagawa, M., Fung, S. Y., Onishi, N., Saya, H. & Lee, S. H. Targeting Aurora B to the equatorial cortex by MKlp2 is required for cytokinesis. *PLoS One* **8,** e64826 (2013).
43. Eilers, M., Picard, D., Yamamoto, K. R. & Bishop, J. M. Chimaeras of Myc oncoprotein and steroid receptors cause hormone-dependent transformation of cells. *Nature* **340,** 66–68 (1989).
44. Morita, T., Kojima, T. & Kitamura, T. Plat-E: an efficient and stable system for transient packaging of retroviruses. *Gene Ther.* **7,** 1063–1066 (2000).

Acknowledgements

We thank T. Hara for the retroviral expression vector pRePS; T. Kitamura for the retroviral expression vector pMXs-puro; O. Sampetrean, S. Kuninaka, and H. Naoe for discussion; RM. Yonamine, X. Wang, H. Ito, N. Yanagihara, and N. Hirose for technical assistance; and K. Arai for secretarial assistance. We are grateful to the Collaborative Research Resources, School of Medicine, Keio University for technical support and reagents. This work was partly supported by a grant from the Ministry of Education, Science, Sports, and Culture of Japan (HS) and a grant from Okinawa Research and Industrialization for the Forefront Medical Care (KK).

Author contributions

H.N. performed most of the experimental works and wrote the manuscript. N.O. helped experimental design and contributed to the writing of the manuscript. T.S., E.S., Y.O., Y.S., T.C and K.A. helped with the experiments and to review the manuscript prior to submission. H.S. and K.K. supervised the project and manuscript editing, and prepared the manuscript.

Additional information

Accession codes: The raw and processed microarray data have been deposited in the Gene Expression Omnibus under the accession code GSE52334.

Supplementary Information accompanies this paper at http://www.nature.com/naturecommunications

Competing financial interests: The authors declare no competing financial interests.

Reprints and permission information is available online at http://npg.nature.com/reprintsandpermissions/

How to cite this article: Nobusue, H. *et al.* Regulation of MKL1 *via* actin cytoskeleton dynamics drives adipocyte differentiation. *Nat. Commun.* 5:3368 doi: 10.1038/ncomms4368 (2014).